Intestinal lamina propria supports acquired eTreg suppressor function

Yisu Gu*[1], Raquel Bartolomé-Casado*[2,3], Chuan Xu[2], Alina Janney[1], Cornelia Heuberger[1], Claire Pearson[1], Sarah Teichmann[3,4], Emily E Thornton*[5,6], Fiona Powrie*[1]
***equal contribution**

[1]Kennedy Institute of Rheumatology, NDORMS, University of Oxford
[2]Wellcome Sanger Institute, Wellcome Genome Campus, Hinxton, Cambridge
[3]Department of Pathology, Oslo University Hospital – Rikshospitalet, Oslo, Norway
[4]Theory of Condensed Matter, Cavendish Laboratory, Department of Physics, University of Cambridge, Cambridge
[5]MRC Human Immunology Unit, MRC Weatherall Institute of Molecular Medicine, University of Oxford
[6]Nuffield Department of Medicine, University of Oxford
[*]these authors contributed equally

Abstract

The intestinal immune system must maintain tolerance to commensal microbiota and self antigens whilst defending against invading pathogens. Recognising how homeostasis is established and maintained in a complex immune environment such as the gut is critical to understanding how to re-establish tolerance once broken in inflammatory disorders. Peripherally induced regulatory T cells (Tregs) play a key role in homeostasis. In intestinal tissue, Tregs work in concert with a diverse network of cells but which cellular interactions occur to instruct Treg adaptation and acquisition of distinct Treg suppressor function is not clear. We used two-photon *in vivo* live imaging and NICHE-seq [1] to deep phenotype *Helicobacter hepaticus* (*Hh*)- specific Tregs with shared specificity but distinct spatially compartmentalised functions in the tissue. We show transcriptionally distinct central Treg (cTreg) and effector Treg (eTreg) populations in lymphoid versus gut tissue. The lamina propria (LP), and not embedded lymphoid aggregates (LA), is the key location of acquired immune suppressor eTreg function. Tregs recruited to the LP compartment are the dominant interacting cell type and acquired a more effector Treg profile with upregulation of *Areg*, *Gzmb, Icos, Tigit, Tnfrsf4* (OX40), and *Tnfrsf18* (GITR). We identify IL-1β^{+} macrophages, CD206+ macrophages, and ILC2 in the LP niche as the key players governing Treg survival and function. In contrast, LA, dominated by interactions with ILC3s and populations of IL-6^{+} DCs, are equipped to tip the balance towards a pro- inflammatory response. By functionally isolating the gut tissue from secondary lymphoid organs, we show that eTregs maintain their phenotype in the context of inflammatory insult. Blocking their key effector molecule, IL-10, results in locally differentiated Th17 cell proliferation without overt inflammation due to local IL-10 independent mechanisms that constrain inflammation. Our results reveal a previously

39 unrecognised spatial mechanism of tolerance, and demonstrate how knowledge of local
40 interactions can guide cell function and potentially be manipulated for the next generation of
41 tolerance-inducing therapies.
42

43 ## Results

44

45 The pathobiont *Helicobacter hepaticus* (*Hh*) establishes life-long infection in the cecum of
46 normal mice. A key host adaptation ensuring immune homeostasis in the face of chronic
47 infection is the production of IL-10 by Tregs [2-4]. Maladaptation of this response results in
48 colitis in mice, and similar processes are thought to underlie very early onset inflammatory
49 bowel disease (VEO-IBD) with deficiencies in the IL-10 pathway a major cause [5]. The MLN
50 has been shown to be a key site of Treg induction [6], but the key anatomical location for
51 induction and maintenance of effector Treg suppressor function is yet to be elucidated. We
52 used HH7-2tg T cells [7] (TCR^{Hh}) in *Hh* colonised hosts to follow the natural history of
53 antigen-specific T cells experiencing key interactions and gaining and sustaining Treg effector
54 functions in the tissue microenvironment.
55
56 To map where adaptive responses to *Hh* occur, we characterised the intestinal lymphoid and
57 non-lymphoid tissue compartments of WT C57BL/6 mice. Lymphoid tissue comprised,
58 secondary lymphoid organs (SLO) including mesenteric lymph nodes (MLN), the caecal patch
59 (CP) and distal colon organised lymphoid structures (OLS) (Fig 1a). Small lymphoid
60 aggregates (LA) are present in the caecum and proximal colon. LA do not have organised T
61 and B-cell zones, and contain a spectrum of tissue organisation from cell aggregates to
62 cryptopatches and isolated lymphoid follicles (ILF) (Supp Fig 1a-c). Previous tracking of naïve
63 TCR^{Hh} *in vivo* showed differentiation to Rorγt^{+} Foxp3^{+} Tregs in colons, but that work did not
64 exclude OLS from the analysis [7]. We sought to understand the natural history of TCR^{Hh} to
65 *Hh* in the context of lymphoid and non-lymphoid compartments, referring to the 'tissue' as the
66 composite of the lamina propria (LP) and the lymphoid aggregates (LA), but exclusive of OLS.
67
68 Naive TCR^{Hh} transferred into *Hh*- colonised hosts (Fig 1b and Supp Fig 1d) home to the SLOs
69 within 24 hours and onwards to the tissue approximately 1 week later (Fig 1c-d). Co-transfer
70 of congenically marked TCR^{Hh} and TCR^{Hh} *Rag1*$^{-/-}$ cells confirmed no effect of endogenous
71 TCRα rearrangement (Supp Fig 2a-d). Further, TCR^{Hh} were not detected in un-colonised hosts,
72 demonstrating their dependence on cognate antigen for survival (Supp Fig 2e). To pinpoint

where important cellular interactions and activation steps take place, we quantified proliferation, Treg differentiation, TCR signalling and IL-10 production across the tissue compartments. Despite early activation in lymphoid tissues (Supp Fig 2f), at 14 days after transfer, tissue TCR^{Hh} cells are more proliferative than their lymphoid counterparts (Fig 1e), and a larger proportion of TCR^{Hh} cells differentiated into Foxp3+ Tregs (Fig 1f) within tissue than SLOs.

As Treg suppressor function has been shown to depend on the T cell receptor (TCR) [8], we wondered whether ongoing TCR stimulation also occurs in TCR^{Hh} in any of the defined tissue microenvironments. Transfer of naïve T cells from TCR^{Hh} crossed to $Nur77^{GFP}$ mice [10] (TCR^{Hh} $Nur77^{GFP}$) into *Hh*-colonised hosts showed the proportion expressing GFP and GFP MFI as a measure of TCR signalling to be highest in the tissue at 11 days post transfer (Fig 1g). Transfer of TCR^{Hh} crossed to B6.$Foxp3^{hCD2}$ IL-10^{GFP} reporter mice [9] (TCR^{Hh}IL-10^{GFP}) also revealed the tissue as the site of the highest proportion of IL-10^{+} TCR^{Hh} cells (Fig 1h). To determine whether TCR engagement and IL-10 production were due to local stimulation, we used the sphingosine 1-phosphate receptor agonist FTY720 to block lymph node egress following TCR^{Hh} recruitment into the gut to ensure detection of local GFP induction (Supp Fig 3a-c). Again, the strongest TCR signalling and highest IL-10 production was detected in tissue TCR^{Hh} cells, which were on par with controls (Supp Fig 3d-g). Absolute numbers of tissue TCR^{Hh} were comparable between FTY720 treated and controls, suggesting local proliferation of TCR^{Hh} (Supp Fig 3h). These data point to the gut tissue as the dominant site of ongoing Treg activation and effector function in the maintenance of tolerance to the pathobiont *Hh*. In fact, lymphotoxin-α deficient mice ($LT\alpha^{-/-}$) that are devoid of MLNs, CP, OLS and LA (Supp Fig 4a-b, and data not shown) [10] still supported TCR^{Hh} homing into the tissue (Supp Fig 4c-e). However, in the absence of lymph nodes, TCR^{Hh} did not differentiate into Tregs (Fig 1i), indicating a non-redundant role for SLOs in Treg differentiation. TCR^{Hh} cells in $LT\alpha^{-/-}$ hosts retained the ability to make IL-10 in similar absolute numbers, albeit at a lower frequency compared to controls (Fig 1j-k, Supp Fig 4f). These data show SLOs are critical for Treg induction, but interactions in the tissue can induce non-Treg TCR^{Hh}IL-10 production independent of SLOs and prevent colitis (Supp Fig 4g).

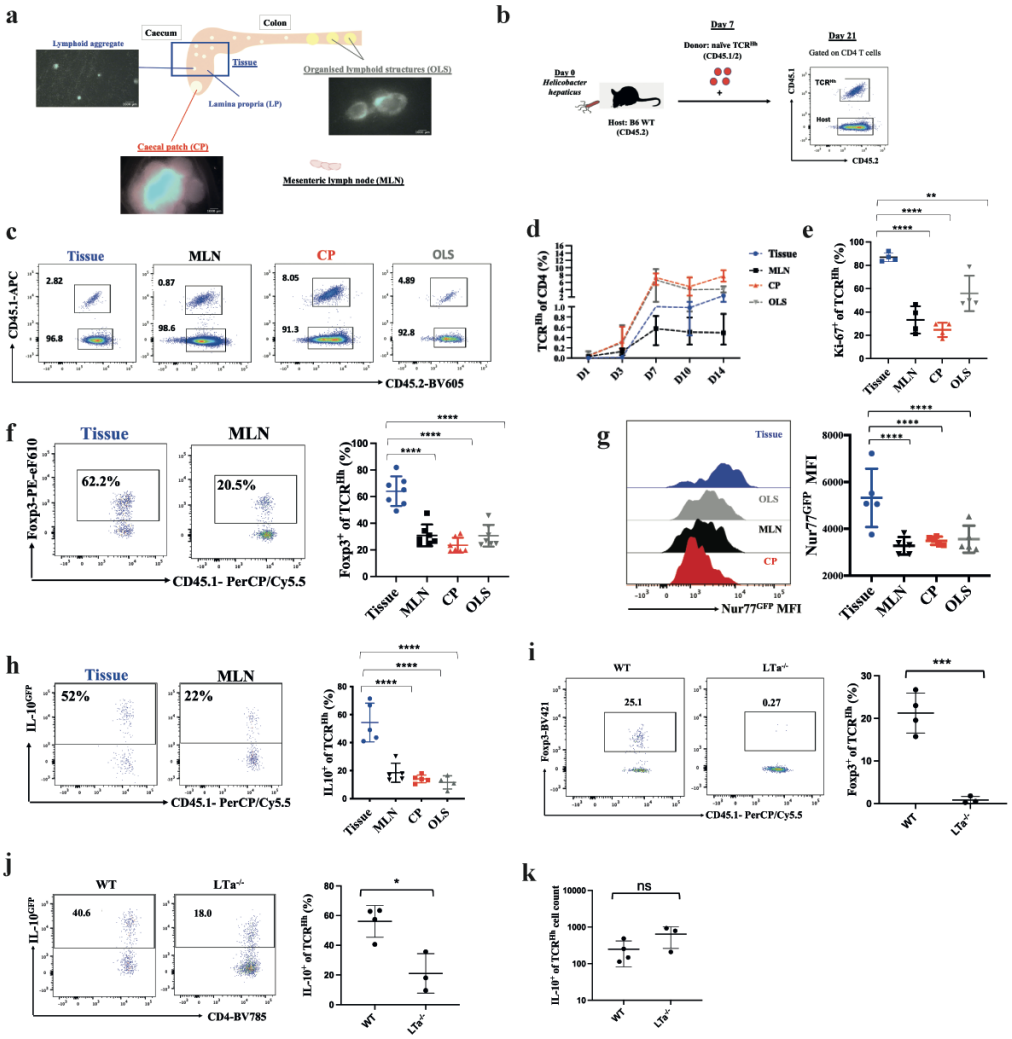

Figure 1. Colon tissue supports the highest IL10 production and strongest TCR signalling in response to *Helicobacter hepaticus*.

a. Diagram of tissue and lymphoid structures in the murine gut, with representative images of caecal patch (CP), organised lymphoid structures (OLS) and lymphoid aggregates (LA) in hCD2-DsRed mouse (scale bar 1000µm).
b. Transfer of naïve CD45.1^{+} TCR^{Hh} T cells into *Hh*-colonised hosts.
c. Representative FACS of T TCR^{Hh} 14 days post transfer at the indicated sites.
d. Frequency of TCR^{Hh} among total CD4 T cells at indicated time points post transfer.
e. Frequency of Ki-67^{+} of TCR^{Hh} at 14 days post transfer at the indicated sites.
f. Representative FACS and frequency of Tregs of TCR^{Hh} at 14 days post transfer.
g. Representative histogram overlay and GFP MFI of TCR^{Hh}Nur77^{GFP} 11 days post transfer.
h. Representative FACS and frequency of IL-10^{+} among TCR^{Hh}IL-10^{GFP} 11 days post transfer.
i. Representative FACS and frequency of Tregs among TCR^{Hh} in tissue of WT and LTα$^{-/-}$ hosts at 10 days post transfer.
j. Representative FACS and frequency of IL-10^{+} among TCR^{Hh} in tissue of WT and LTα$^{-/-}$ hosts at 10 days post transfer.
k. Absolute cell count of IL-10^{+} among TCR^{Hh} in tissue of WT and LTα$^{-/-}$ hosts at 10 days post transfer.

Our results demonstrate tissue interactions play a dominant and previously unrecognised role in TCR stimulation and IL-10 production of microbe-reactive T cells, including Tregs. We next wished to determine if the LP and LA niches played individual roles in shaping the TCR^{Hh} response to *Hh*. We bred TCR^{Hh}Nur77^{GFP} and TCR^{Hh}IL-10^{GFP} to hCD2-DsRed mice

128 [11] (TCR^{Hh} CD2^{Dsred}Nur77^{GFP} or TCR^{Hh} CD2^{Dsred}IL10^{GFP}) and separately transferred naïve T
129 cells from these reporter lines into *Hh*-colonised Foxp3^{GFP} hosts for *in vivo* two-photon live
130 imaging (Fig 2a). Host LA containing Tregs appear as green clusters. Transferred TCR^{Hh} are
131 red, but co-express GFP upon TCR stimulation or IL-10 production. Acquisition in 3-
132 dimensions allows for distinction of green/red co-expression versus two overlapping cells
133 (Supp video 1).
134
135 Within tissue, TCR^{Hh}Nur77^{GFP+} T cells were present within LA (Fig 2b). Surprisingly,
136 TCR^{Hh}Nur77^{GFP+} cells were also located within the LP, spatially distant from LA (Fig 2b).
137 This even distribution of recently activated T cells (Fig 2c) suggest TCR-MHCII interactions
138 occur between TCR^{Hh} and LP- resident APCs, and/or rapid migration of TCR-stimulated
139 TCR^{Hh} out of LA into LP after TCR engagement. Indeed, time-lapse videos reveal
140 TCR^{Hh}Nur77^{GFP+} cells to be highly motile (Supp video 2). We next wondered which tissue
141 niche supported the highest production of IL-10 [12]. *In vivo* live imaging of donor TCR^{Hh}
142 CD2^{Dsred}IL10^{GFP} in *Hh*-colonised Foxp3^{GFP} hosts demonstrated that IL-10 production by
143 TCR^{Hh} cells was largely restricted to the LP (Fig 2b-c). IL-10^{+} TCR^{Hh} cells were actively
144 motile throughout the tissue (Supp video 3), suggesting far-reaching suppressor function in
145 response to *Hh*.
146
147 Because TCR^{Hh} cells that have recently experienced TCR stimulation are distributed
148 throughout the LP and LA niches, whereas production of the Treg effector molecule IL-10 is
149 highest in the LP niche, we wondered which cellular interactions and/or molecular cues in the
150 LP niche drive TCR^{Hh} activation and Treg effector functions. We used two-photon
151 photoactivation labelling of cells within T cell niches followed by scRNA-seq (NICHE-seq)
152 to uncover transcriptional states and cellular composition of tissue microniches [1, 13]. Naïve
153 T cells from TCR^{Hh} CD2^{Dsred} crossed to ubiquitously expressing photoactivatable GFP mice
154 (TCR^{Hh} CD2^{Dsred}Ub^{PA-GFP}) [13] were transferred into *Hh*-colonised CD2^{Dsred}Ub^{PA-GFP} hosts so
155 both host and donor cells were photoactivatable. DsRed was used to visualise donor cells,
156 and to mark T cell zones in host lymphoid tissue. We used two-photon microscopy to label
157 donor and host cells with photoactivated GFP from four regions: the T cell zones of MLNs
158 and CP, the LA and LP (Fig 2d-e and Supp Fig 5a). scRNAseq of GFP+ cells was performed
159 using 10X and 5' GEX and VDJ TCR sequencing.
160

161 A model built on previously published work [14-21] supported annotation of a spectrum of
162 myeloid cells, T cells, ILCs, B cells, plasma cells, epithelial cells, mesenchymal cells,
163 endothelial cells, and granulocytes across all 4 sites (Fig 2f-g, Supp Fig 5b, Supp Fig 6-7, and
164 Supp Table 1). The relative distributions of these major intestinal cell types differ according
165 to region, with a sizeable T cell population present in all micro-niches (Fig 2g). To
166 understand how location affects suppressor function, we focussed on the lymphoid and
167 myeloid populations in each niche that have the potential to form meaningful interactions
168 with TCR^{Hh}.

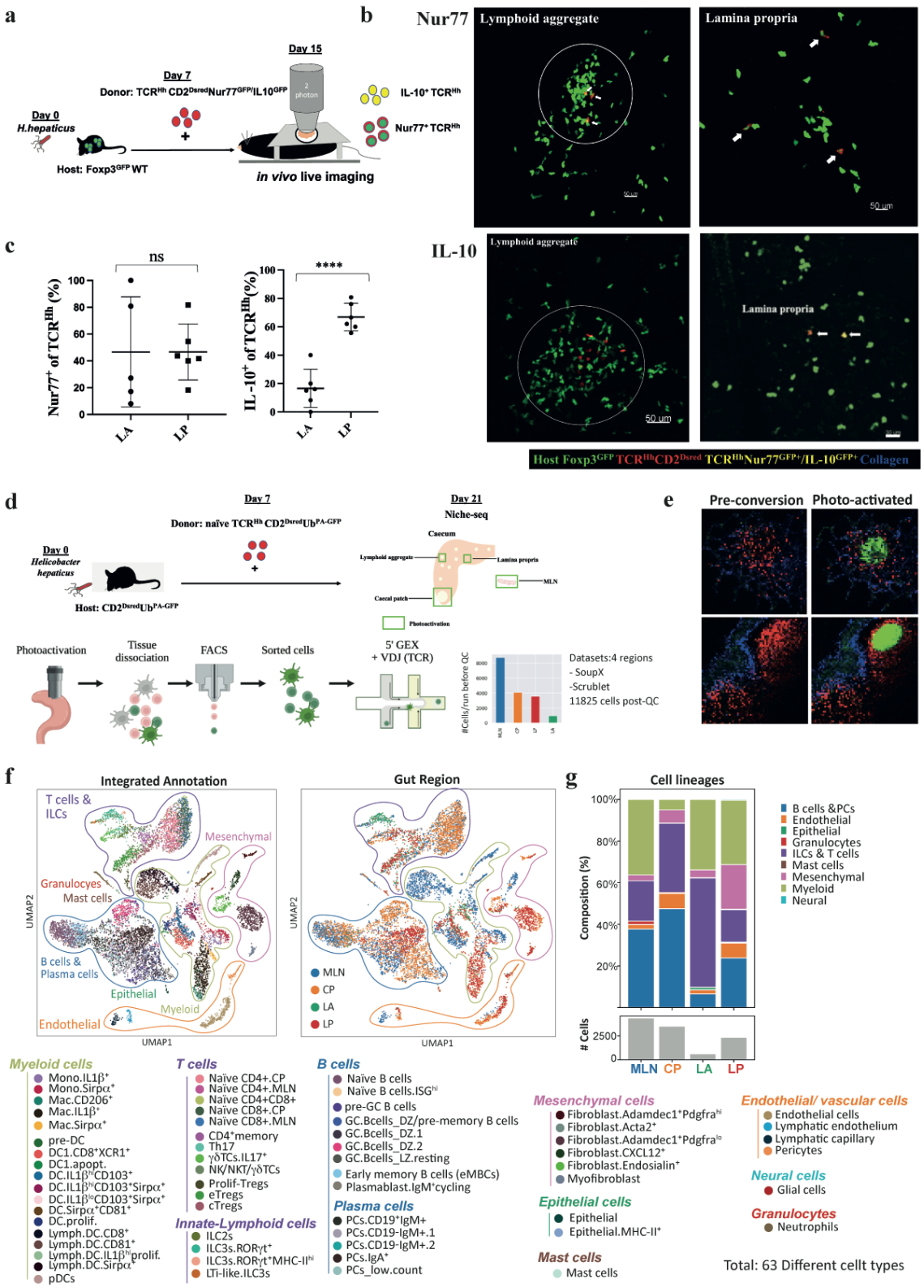

Figure 2. IL-10 production by TCR^{Hh} is enriched in the LP, and NICHE-seq allows identification of cellular composition across T cell microniches

a. Two photon *in vivo* live imaging of transferred naive TCR^{Hh}CD2^{dsRed}Nur77^{GFP} or TCR^{Hh}CD2^{dsRed}IL-10^{GFP} into *Hh*-colonised Foxp3^{GFP} hosts.

b. Representative images of $TCR^{Hh}Nur77^{GFP}$ cells (top panels) and $TCR^{Hh}IL\text{-}10^{GFP}$ (bottom panels) in the lymphoid aggregates (LA) and lamina propria (LP). TCR^{Hh} $Nur77^{GFP}/IL\text{-}10^{GFP}$ positive cells indicated by white arrowheads.
c. Frequency of $Nur77^{GFP}$ (left) and $IL\text{-}10^{GFP}$ (right) positive of TCR^{Hh} in the LA and LP.
d. NICHE-seq of gut tissue: Transfer of $TCR^{Hh}CD2^{Dsred}Ub^{PA\text{-}GFP}$ into $CD2^{Dsred}Ub^{PA\text{-}GFP}$ hosts with subsequent photo-activation, cell sorting and scRNA-seq. Numbers of single cells acquired before and after QC as indicated.
e. Representative images of pre- and post-photoactivation of the LA (top panels) and T cell zone of CP(bottom panels) of $CD2^{Dsred}Ub^{PA\text{-}GFP}$ hosts.
f. UMAP visualisation of total cell subsets and detailed cell type annotations in each cell lineage (left) and their distribution in each gut location (right).
g. Bar chart showing cell subsets and total cell numbers at the indicated gut locations.

The T/ILC compartment comprises 16 transcriptionally distinct subsets (Fig 3a). As expected, naïve $CD4^+$ and $CD8^+$ T cells were mainly located in the MLNs and CP. ILC3s were dominant in the LA and ILC2s in the LP. The LP also contained a sizeable population of memory CD4 T cells. As suggested by the imaging data, Tregs were enriched in both LP and LA.

Subclustering of Tregs revealed 3 subpopulations that are differentially distributed between SLOs and the tissue (Fig 2b). Lymphoid Tregs express *Tcf7* and *Ccr7* [22, 23], tissue Tregs express effector-associated molecules *Ctla4*, *Maf and Tnfrsf4*, and proliferating Tregs express histone genes (Fig 3b) [7, 24]. To highlight their distinct functional phenotype and spatial segregation, we refer to lymphoid associated Tregs as central Tregs (cTregs) and tissue resident Tregs as effector Tregs (eTregs).

To determine whether the host and transferred cells were comparable for downstream analysis, we performed a T cell clonotype analysis. TCR repertoire sequencing revealed the TCR^{Hh} clone (clonotype 554 and 249) as well as many host clonotypes to be present in all four regions and predominantly differentiate into the eTreg phenotype (Fig 3c). Host and TCR^{Hh} Tregs had similar mean expression of classical suppressor genes such as *Ctla4, Tigit,* and *Il10* (Supp Fig 8a), allowing combination of clonotypes for further analysis.

We next examined myeloid APC subset(s) across the tissue microniches, focusing especially on cells that may affect eTreg function in the tissue [25]. Mapping of monocyte/macrophage and dendritic cell subsets across the 4 regions did not reveal a unique APC population (Fig 3d); however, we identified an enrichment of $IL\text{-}1\beta^{hi}CD103^+Sirp\alpha^+$ dendritic cells within LA, whilst $IL\text{-}1\beta^+$ and $CD206^+$ macrophages and IL-1β+ monocytes were most abundant in the LP (Fig 3e).

214 By comparing APC populations present at >30 cells per microniche, we could see MHCII score
215 for LP-resident IL-1β^{+} macrophages was comparable to IL-1β^{hi}CD103^{+} and IL-
216 1β^{hi}CD103^{+}Sirpα^{+} dendritic cells (Fig 3f, gene list: Supp Table 2). Taking abundance and
217 MHCII expression into consideration, IL-1β^{+} macrophages dominate the T cell activation
218 landscape in the LP, whilst IL-1β^{hi}CD103^{+}Sirpα^{+} dominate in the LA. MHCII^{+} ILC3s have
219 been shown to regulate CD4^{+} T cell responses to gut commensals and maintain homeostasis in
220 the MLN [26, 27]. LA are enriched for ILC3s, with a small subset expressing MHCII; however,
221 this is a smaller fraction than present in the MLN (Fig 3f and Supp Fig 8b).
222
223 After defining the cellular composition, we sought to understand the potential cellular
224 interactions at each location. We performed CellPhoneDB analysis [28] to understand the
225 interactions between eTregs and T/ILC/myeloid cells for each tissue micro-niche based on
226 populations with greater than 30 cells present. In the LP, eTregs are capable of interacting with
227 all cell populations within the niche with many potential interactions across APC subsets (Fig
228 3g). This fits with their dynamic nature as observed previously with intravital microscopy
229 (Supp video 3). LA interaction diagram demonstrates eTregs have more interactions with IL-
230 1β+CD103+Sirp1α+ DCs, in particular (Fig 3g).
231
232 CellPhoneDB analysis of LA and LP catalogue key interactions between cells in each tissue
233 microniche. Of particular interest are the chemokine/chemokine receptor pairs that bring APCs
234 and eTregs together, TGFβ, and cell-cell contact molecules, which all differ between LP and
235 LA (Fig 3h). Within the LP microniche, eTregs have the strongest *Ccr2*/*Ccl8* (Supp Fig8c),
236 *Ptprc*/*Mrc1*, and *Csf1*/*Csfr1* pathway interactions with CD206 macrophages suggesting these
237 cells may play a dominant role beyond TCR engagement. Within the LA microniche, the
238 *Ccr2*/*Ccl8*, *Ptprc*/*Mrc1*, and *CD72*/*Sema4d* instead connect eTregs with IL-1β+ macrophages,
239 and *Cxcr3*/*Cxcl9*, *Icam1*/*Itgal* interactions connect eTregs with LA DC populations. In addition
240 to differences in interactions with APCs, the eTregs in the LP had the strongest *Icam1*/*Itgal*
241 interactions with CD4 memory T cells and *Ltbr*/*Ltb* interactions with ILC2s whereas eTregs in
242 the LA could interact with ILC3s through *Icam1*/*Itgal* (Fig 3h).

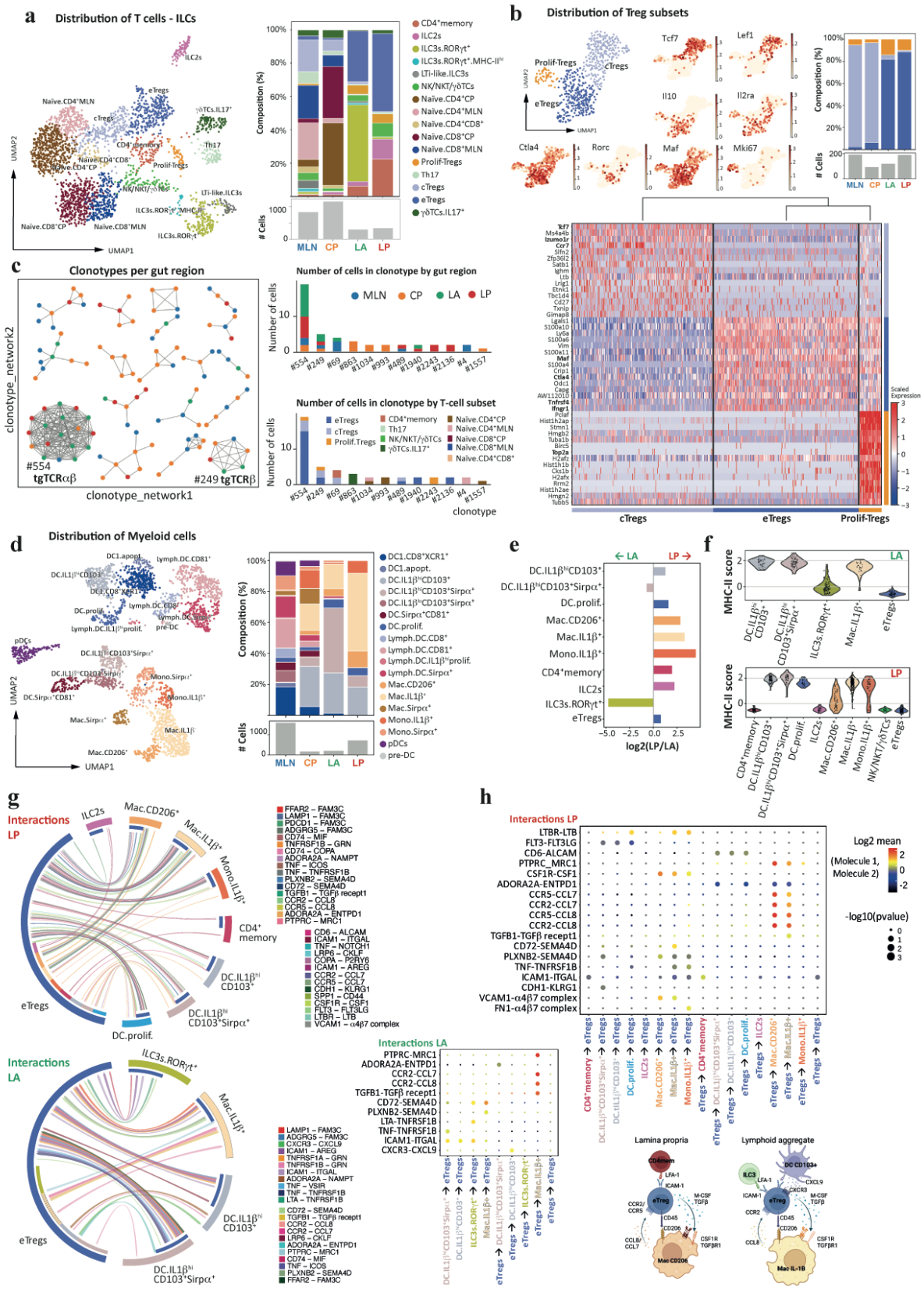

Figure 3. Lymphoid and myeloid cell subset data highlight distinct interactions in LP and LA microniches

a. UMAP visualisation of lymphoid subsets across all locations (left). Bar chart showing distribution of lymphoid subsets and cell numbers for each gut location (right). Total cell numbers at the indicated locations (bottom right).

b. UMAP visualisation of Treg subsets across all locations (top left) and overlay on the UMAP plot of the expression of selected genes (centre). Bar chart showing the distribution of Treg subsets and total cell numbers at the indicated locations (right). Heatmap of differentially expressed genes in the indicated Treg subsets across all locations (bottom).
c. Visualisation of clonotype network analysis of TCR clones (left). Barchart showing the distribution of TCR clones by gut location (right top) and T cell subset (right bottom).
d. UMAP visualisation of total myeloid subsets across all locations (left). Bar chart showing myeloid subsets and total cell numbers at the indicated locations (right).
e. Bar plot showing the fold change (log2) of proportions for myeloid, T cells and ILCs between LP and LA.
f. Violin plots of MHC-II expression score across lymphoid and myeloid cells in the LA and LP (restricted to cell types with >30 cells per region).
g. Chord diagrams showing significant interactions of Tregs with lymphoid and myeloid cells, separately for each gut location, LP (left) and LA (right), restricted to cell types with >30 cells per region.
h. CellPhoneDB analysis of receptor/ligand interactions in the LP (top) and LA (centre), restricted to cell types with >30 cells per region and excluding MHC-II interactions. Schematic summarising the most relevant cell-cell interactions (bottom).

Based on our imaging data (Fig 2b-c) and the differences in cell interactions within the tissue microniches, we suspected the LP and LA eTregs would have additional phenotypic differences. By comparing the eTreg populations across the tissue micro-niches, we found upregulation of *Gzmb, Areg, Ccr2,* and *Il2ra* in the LP microniche and *Cxcr4* in the LA (Fig 4a) [29, 30]. This highlights the LP as a key site that favours optimal eTreg function. This was also supported by mean expression data of known Treg effector molecules showing increases in *Areg*, *Gzmb, Icos, Tigit,* and *Tnfrsf18* (GITR) in the LP (Fig. 4a). Velocity pseudotime analysis of eTreg, cTreg, and proliferating Tregs suggests a trajectory of eTregs from MLN/CP to LA and on to LP with proliferating Tregs more closely related to eTregs (Fig 4b and Supp Fig8d-e). This raises questions about whether LP eTregs are terminally differentiated or whether these cells are plastic and capable of proliferating *in situ*.

With all the data pointing to unique interactions and enhanced eTreg functions in the LP niche, we wanted to determine whether key known pathways such as survival cytokines and upregulators of Maf, TGFβ and STAT-3 cytokines, [14, 31, 32] are also spatially segregated within the tissue microniches. To understand which survival cytokines are required in the LP niche, we looked at receptors for gamma-chain cytokines on our Treg populations of interest. eTregs in the LP and LA express *Il2r* with highest expression in the LP microniche (Fig 4c). To determine which are the important cells that produce IL-2, we looked for expression in the cells present in the tissue. ILC2 and CD4 memory cells are the dominant sources of IL-2, with both populations present in the LP microniche and shown to have potential for interactions with eTregs in the LP (Fig 4c and Fig 3g).

289 TGFβ is widely expressed by most myeloid and lymphoid populations, including eTregs in the
290 LA and LP (Fig 4d). However, eTregs in the LP are one of the few tissue populations that also
291 express high levels of *Itgav* as well as *Itgb8* (Fig 4d), encoding the integrin subunits alpha V
292 and beta 8 that are required to activate latent TGFβ [33]. This activated TGFβ can act in an
293 autocrine and paracrine manner to control local immune responses, which is required for
294 immune homeostasis [34, 35]. We next performed a comprehensive search of STAT3-
295 dependent cytokine genes across the most abundant myeloid and lymphoid subsets in the tissue.
296 We found upregulated gene expression of the pro-inflammatory cytokine *Il6* in IL-
297 $1\beta^{+}$CD103^{+}Sirpα^{+} DCs resident in the LA (Fig 4e). In contrast, the LP was dominated by *Il10*,
298 expressed primarily by eTregs with some expression in CD206^{+} and IL-1β^{+} macrophage
299 subsets (Fig 4e). A small amount of *Il27* could be detected in the IL-1β^{+} macrophage
300 population, specifically in the LP. Together these data establish myeloid cytokine microniches
301 capable of tuning STAT-3 signals, potentially establishing inflammatory (LA) and anti-
302 inflammatory (LP) niches within the intestinal tissue. We next examined expression levels of
303 cytokine receptors. Moderate levels of *Il6ra* can be detected across myeloid populations, and
304 *Il27ra* expression is largely restricted to eTreg, CD4+ memory T cells, and ILC2 populations.
305 *Il10ra* is highly expressed on CD206^{+} and IL-1β^{+} macrophages and IL-1β^{+} monocytes,
306 especially in the LP niche (Fig 4e). Macrophage sensing of IL-10 is critical for gut homeostasis
307 [36, 37], and this data supports a positive feedback loop in the LP. CD206^{+} and IL-1β^{+}
308 macrophages respond to IL-10 and produce IL-10 and IL-27 [38, 39], activating STAT3 and
309 supporting the *Maf* program in eTregs in the LP. This raises the question of whether acute
310 perturbation of the IL-10 pathway could disrupt the LP eTreg phenotype and function.
311
312 After identifying spatially separated cTreg and eTreg responses to *Hh* and enhanced eTreg
313 suppressor function within the LP, we sought to determine whether an inflammatory challenge
314 that interferes with IL-10, a key eTreg effector molecule in the LP microniche, can affect eTreg
315 phenotype or proliferation. We transferred TCR^{Hh} into colonised hosts as before. TCR^{Hh}
316 migrate to the gut 7 days after transfer and adopt an IL10^{+} Treg fate (Fig 1d, f and h). To isolate
317 the interactions in the gut tissue niches from the SLOs, FTY720 was injected daily from day
318 8, resulting in a pool of TCR^{Hh} cells trapped in the tissue (Fig 4f). We subsequently disrupted
319 the IL10 positive feedback loop with an IL10Rα blocking antibody 10 days after cell transfer.
320 Flow cytometry analysis validated NICHE-seq RNA expression of *Tcf7* in cTregs and *Maf*
321 expression in eTregs (Fig 4g). At 3 days after anti-IL10Rα treatment (13 days after TCR^{Hh} cell

322 transfer), there was no significant difference between the two treatment groups in terms of
323 TCR^{Hh} Treg proportion or phenotype (Supp Fig 9a). However, by 7 days after anti-IL10Rα
324 treatment (17 days after TCR^{Hh} cell transfer), there was an increase in local proliferation of
325 TCR^{Hh} and host T cells with approximately 60% of TCR^{Hh} Tregs and Th17s expressing Ki-67
326 (Fig 4h). It has been suggested that eTregs may be terminally differentiated and therefore less
327 able to proliferate; however, proliferating eTregs expressed similar levels of Foxp3 and C-maf
328 compared to controls (Fig 4i and Supp Fig 9b). 7 days after anti-IL10Rα treatment, while we
329 observe some increased cytokine expression, we did not observe overt inflammation (Fig 4j-k
330 and Supp Fig 9c) suggesting that while IL-10 is critical to restrain Th17s, other eTreg
331 suppressor functions are able to constrain the local inflammatory response. To determine which
332 niche in the intestinal tissue supported Treg proliferation in this perturbed environment, we
333 stained tissues with Ki67, Foxp3, and Hoechst. This demonstrated Treg proliferation in the LP
334 niche (Fig 4l-m), again supporting the LP as the key location for eTreg function in the gut.
335 These findings taken together with our Niche-seq data suggest that eTreg suppressor functions
336 (e.g. Tigit, ICOS, and GITR Fig 4a and Supp Fig 10) in the LP can constrain the inflammatory
337 response when the local IL-10 circuit is disrupted.

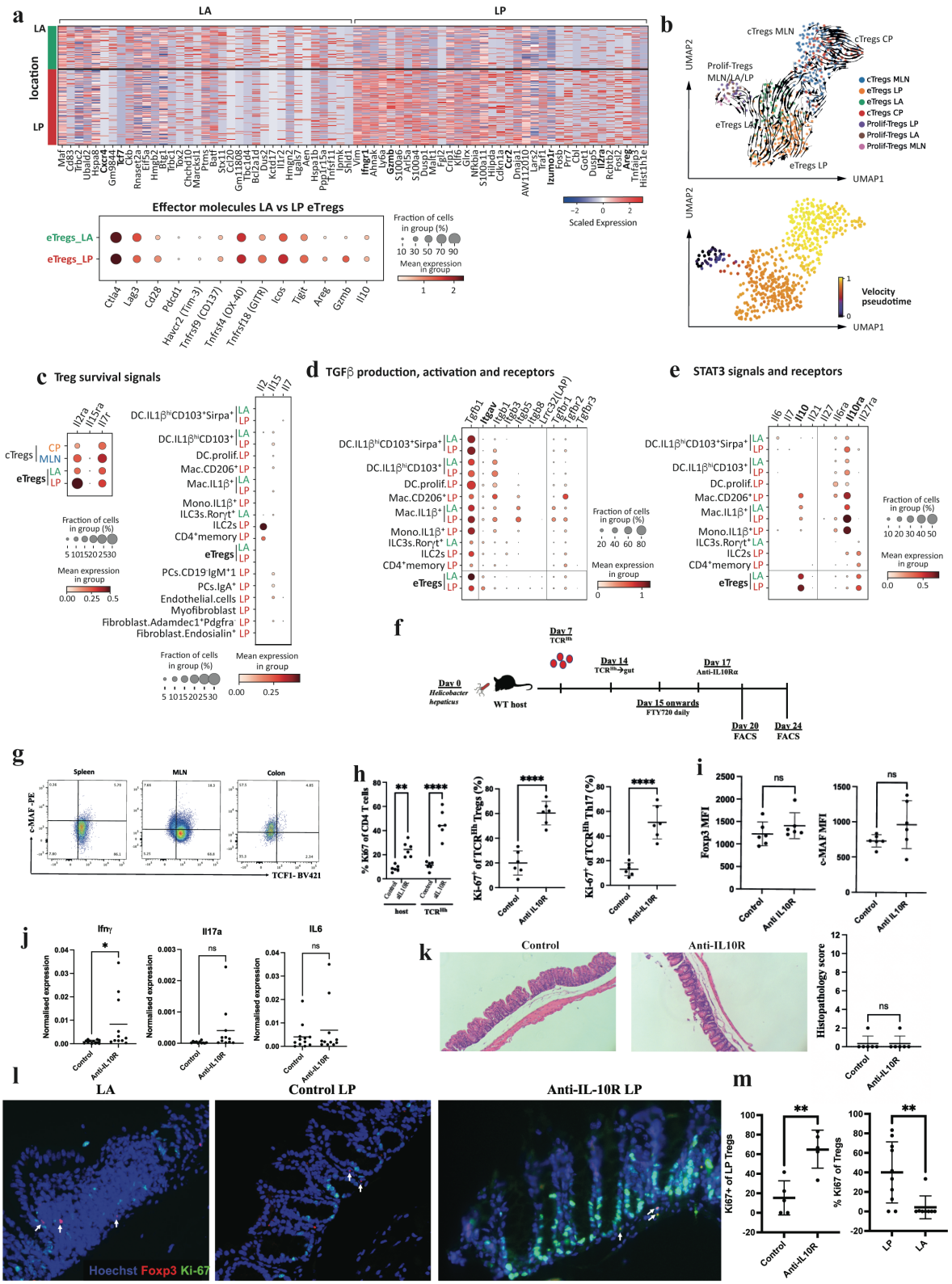

Figure 4. The LP niche promotes eTreg survival, phenotype, and function

a. Heatmap showing differential gene expression of eTregs in the LA *versus* LP (top) and dot plot showing relative expression of selected effector molecule genes within eTregs located in the LA *versus* LP (bottom). **b.** UMAP of Treg subsets per location, filtering out the subsets with less than 10 cells in a given location (i.e. excluding eTregs_MLN, eTregs_CP, cTregs_LA, cTregs_LP and Prolif-Tregs_CP). Arrows depict summarised

344 scVelo differentiation trajectories (above). Heat map overlay on the Treg UMAP indicating velocity
345 pseudotime, as calculated by scVelo (below).
346 **c.** Dot plot showing relative expression of survival cytokine genes expressed by all the cell types with >30 cells
347 in LA or LP regions (right) and their receptors in Treg populations (left).
348 **d.** Dot plot showing relative mean expression of TGF-β and its associated receptor and activating integrin genes
349 in the main myeloid and lymphoid subsets (>30 cells per region) in the LA and LP.
350 **e.** Relative mean expression of STAT3 signalling genes and receptors within main myeloid and lymphoid
351 subsets (>30 cells per region) in the LA and LP.
352 **f.** TCR^{Hh} were transferred into *Hh* colonised host mice, treated with daily FTY720 from day 15 and anti-IL-
353 10Rα at day 17.
354 **g.** FACS validation of c-MAF and TCF1 protein expression in spleen, MLN and tissue sites of host Tregs at day
355 20 post *Hh* infection.
356 **h.** Ki-67 of total CD4 T cells of TCR^{Hh} and host cells (left), Ki-67 of TCR^{Hh} Tregs (centre) and Ki-67 of TCR^{Hh}
357 Th17 cells (right) in control and anti-IL-10Rα treated mice at day 24.
358 **i.** MFI of Foxp3 (left) and c-MAF (right) of TCR^{Hh} Tregs from control and anti-IL10Rα treated mice at day 24.
359 **j.** Expression of *Ifng*, *Il17a* and *Il6* in caecum tissue by qPCR in control and anti-IL10Rα treated mice at day 24
360 **k.** Representative H and E staining (left) and histopathology score (right) of caecum tissue from control and
361 anti-IL10Rα treated mice at day 24.
362 **l.** Representative immunofluorescent staining of Foxp3 and Ki-67 in LA (left panel, arrows mark Ki-67 negative
363 Tregs), control LP (centre, arrows mark Ki-67 negative Tregs), and anti-IL10Rα treated LP (right panel, arrows
364 mark Ki-67 positive Tregs).
365 **m.** Frequency of Ki-67 positive Tregs in the LP of control and anti-IL10Rα treated mice (left) and frequency of
366 Ki-67 positive Tregs in the LP and LA in both control and anti-IL10Rα treated mice (right).
367

368 ## Discussion

369

370 In this study, we follow the natural history of microbe-reactive Tregs as they acquire and
371 maintain immune regulatory function in the intestine. By examining cells in anatomical
372 microniches, we have revealed spatial diversity of cTreg and eTreg subsets in lymphoid and
373 non-lymphoid tissues and the importance of the lamina propria niche, not the lymphoid
374 aggregates, as the site of enhanced eTreg function. The LA microniche may act as an entry
375 point for eTregs into the tissue with the potential to skew the response toward inflammation
376 through eTreg interactions with DCs and ILC3s. The LP niche is unique in its myeloid cell
377 makeup with interactions between macrophages and eTregs through antigen presentation,
378 CCR2/CCL8, CD45/CD206, and IL10/IL10R axes contributing to recruitment of highly motile
379 eTregs and fine tuning of the immune response to pathobiont colonization.
380

381 By perturbing the system with IL-10Rα blocking antibodies, we demonstrate that eTregs are
382 able to maintain their c-Maf and Foxp3 levels while proliferating in LP niche in the context of
383 an inflammatory milieu. While IL-10Rα blockade results in proliferation of Th17 cells, colitis
384 does not develop, likely due to additional eTreg effector molecules including GITR, Tigit,
385 CTLA-4, and granzymeB that remain intact.
386

387 Cell therapy and vaccination strategies to promote and establish tolerance in inflammatory
388 diseases will rely on Tregs that can function in inflammatory conditions, and we provide
389 support for eTregs as an ideal therapeutic population, capable of maintaining their phenotype
390 in an inflammatory milieu. Information gained from the study of microniches can be used for
391 targeted interventions to support eTreg recruitment, activation, differentiation, survival and
392 function in the inflammatory niche within the intestine and beyond.

1. Medaglia, C., et al., *Spatial reconstruction of immune niches by combining photoactivatable reporters and scRNA-seq.* Science, 2017.
2. Kullberg, M.C., et al., *Bacteria-triggered CD4(+) T Regulatory Cells Suppress Helicobacter hepaticus–induced Colitis.* The Journal of Experimental Medicine, 2002. **196**(4): p. 505-515.
3. Hue, S., et al., *Interleukin-23 drives innate and T cell-mediated intestinal inflammation.* J Exp Med, 2006. **203**(11): p. 2473-83.
4. Kullberg, M.C., et al., *IL-23 plays a key role in Helicobacter hepaticus–induced T cell–dependent colitis.* The Journal of Experimental Medicine, 2006. **203**(11): p. 2485-2494.
5. Glocker, E.O., et al., *Inflammatory bowel disease and mutations affecting the interleukin-10 receptor.* N Engl J Med, 2009. **361**(21): p. 2033-45.
6. Kedmi, R., et al., *Microbiota-instructed regulatory T cell differentiation is mediated by a distinct RORγt⁺ antigen presenting cell subset.* bioRxiv, 2022: p. 2021.11.19.469318.
7. Xu, M., et al., *c-Maf-dependent regulatory T cells mediate immunological tolerance to intestinal microbiota.* bioRxiv, 2017.
8. Levine, A.G., et al., *Continuous requirement for the TCR in regulatory T cell function.* Nat Immunol, 2014. **15**(11): p. 1070-8.
9. Kamanaka, M., et al., *Expression of interleukin-10 in intestinal lymphocytes detected by an interleukin-10 reporter knockin tiger mouse.* Immunity, 2006. **25**(6): p. 941-52.
10. De Togni, P., et al., *Abnormal development of peripheral lymphoid organs in mice deficient in lymphotoxin.* Science, 1994. **264**(5159): p. 703-707.
11. Veiga-Fernandes, H., et al., *Tyrosine kinase receptor RET is a key regulator of Peyer's Patch organogenesis.* Nature, 2007. **446**(7135): p. 547-551.
12. Fenton, T.M., et al., *Immune Profiling of Human Gut-Associated Lymphoid Tissue Identifies a Role for Isolated Lymphoid Follicles in Priming of Region-Specific Immunity.* Immunity, 2020. **52**(3): p. 557-570.e6.
13. Victora, G.D., et al., *Germinal Center Dynamics Revealed by Multiphoton Microscopy Using a Photoactivatable Fluorescent Reporter.* Cell, 2010. **143**(4): p. 592-605.
14. Xu, M., et al., *c-MAF-dependent regulatory T cells mediate immunological tolerance to a gut pathobiont.* Nature, 2018. **554**(7692): p. 373-377.
15. Kalucka, J., et al., *Single-Cell Transcriptome Atlas of Murine Endothelial Cells.* Cell, 2020. **180**(4): p. 764-779.e20.
16. Haber, A.L., et al., *A single-cell survey of the small intestinal epithelium.* Nature, 2017. **551**(7680): p. 333-339.
17. Drokhlyansky, E., et al., *The Human and Mouse Enteric Nervous System at Single-Cell Resolution.* Cell, 2020. **182**(6): p. 1606-1622.e23.
18. Almanzar, N., et al., *A single-cell transcriptomic atlas characterizes ageing tissues in the mouse.* Nature, 2020. **583**(7817): p. 590-595.
19. Corbin, A.L., et al., *IRF5 guides monocytes toward an inflammatory CD11c⁺ macrophage phenotype and promotes intestinal inflammation.* Science Immunology, 2020. **5**(47): p. eaax6085.
20. Biton, M., et al., *T Helper Cell Cytokines Modulate Intestinal Stem Cell Renewal and Differentiation.* Cell, 2018. **175**(5): p. 1307-1320.e22.
21. Grenov, A., et al., *YTHDF2 suppresses the plasmablast genetic program and promotes germinal center formation.* Cell Rep, 2022. **39**(5): p. 110778.
22. Xing, S., et al., *Tcf1 and Lef1 are required for the immunosuppressive function of regulatory T cells.* Journal of Experimental Medicine, 2019. **216**(4): p. 847-866.

23. Yang, B.-H., et al., *TCF1 and LEF1 Control Treg Competitive Survival and Tfr Development to Prevent Autoimmune Diseases.* Cell reports, 2019. **27**(12): p. 3629-3645.e6.
24. Miragaia, R.J., et al., *Single-Cell Transcriptomics of Regulatory T Cells Reveals Trajectories of Tissue Adaptation.* Immunity, 2019. **50**(2): p. 493-504.e7.
25. Russler-Germain, E.V., et al., *Gut Helicobacter presentation by multiple dendritic cell subsets enables context-specific regulatory T cell generation.* eLife, 2021. **10**: p. e54792.
26. Hepworth, M.R., et al., *Immune tolerance. Group 3 innate lymphoid cells mediate intestinal selection of commensal bacteria-specific CD4$^+$ T cells.* Science (New York, N.Y.), 2015. **348**(6238): p. 1031-1035.
27. Melo-Gonzalez, F., et al., *Antigen-presenting ILC3 regulate T cell–dependent IgA responses to colonic mucosal bacteria.* Journal of Experimental Medicine, 2019. **216**(4): p. 728-742.
28. Jin, S., et al., *Inference and analysis of cell-cell communication using CellChat.* Nat Commun, 2021. **12**(1): p. 1088.
29. Arpaia, N., et al., *A Distinct Function of Regulatory T Cells in Tissue Protection.* Cell, 2015. **162**(5): p. 1078-89.
30. Burzyn, D., et al., *A special population of regulatory T cells potentiates muscle repair.* Cell, 2013. **155**(6): p. 1282-95.
31. Ciofani, M., et al., *A validated regulatory network for Th17 cell specification.* Cell, 2012. **151**(2): p. 289-303.
32. Apetoh, L., et al., *The aryl hydrocarbon receptor interacts with c-Maf to promote the differentiation of type 1 regulatory T cells induced by IL-27.* Nat Immunol, 2010. **11**(9): p. 854-61.
33. Travis, M.A., et al., *Loss of integrin alpha(v)beta8 on dendritic cells causes autoimmunity and colitis in mice.* Nature, 2007. **449**(7160): p. 361-5.
34. Li, M.O., S. Sanjabi, and R.A. Flavell, *Transforming growth factor-beta controls development, homeostasis, and tolerance of T cells by regulatory T cell-dependent and -independent mechanisms.* Immunity, 2006. **25**(3): p. 455-71.
35. Coombes, J.L., et al., *A functionally specialized population of mucosal CD103+ DCs induces Foxp3+ regulatory T cells via a TGF-beta and retinoic acid-dependent mechanism.* J Exp Med, 2007. **204**(8): p. 1757-64.
36. Zigmond, E., et al., *Macrophage-Restricted Interleukin-10 Receptor Deficiency, but Not IL-10 Deficiency, Causes Severe Spontaneous Colitis.* Immunity, 2014. **40**(5): p. 720-733.
37. Shouval, D.S., et al., *Interleukin-10 receptor signaling in innate immune cells regulates mucosal immune tolerance and anti-inflammatory macrophage function.* Immunity, 2014. **40**(5): p. 706-719.
38. Do, J.s., et al., *An IL-27/Lag3 axis enhances Foxp3+ regulatory T cell–suppressive function and therapeutic efficacy.* Mucosal Immunology, 2016. **9**(1): p. 137-145.
39. Do, J., et al., *Treg-specific IL-27Rα deletion uncovers a key role for IL-27 in Treg function to control autoimmunity.* Proceedings of the National Academy of Sciences, 2017. **114**(38): p. 10190-10195.

488 **Author contributions**

489 Yisu Gu designed, performed, and analysed the experiments and prepared the manuscript.
490 Raquel Bartolomé-Casado conceived of and performed the single-cell sequencing analysis and
491 prepared the manuscript. Chuan Xu created the analysis model and assisted with manuscript
492 preparation. Alina Janney performed experiments. Cornelia Heuberger performed experiments.
493 Claire Pearson facilitated and supervised experimentation and provided intellectual input.
494 Sarah Teichmann supervised analysis and manuscript preparation. Emily Thornton designed,
495 performed, and analysed experiments, supervised the project, and prepared the manuscript.
496 Fiona Powrie designed experiments, and supervised the project and manuscript preparation.
497
498

499 **Acknowledgements**

500 We would like to thank the Kennedy Institute of Rheumatology (KIR) Flow Cytometry Facility
501 and the manager, Jonathan Webber, for help with flow cytometry and FACS, the KIR
502 Biomedical Services Unit, especially Luke Barker for help with animal care and husbandry,
503 and the KIR microscopy facility and manager Christoffer Lagerholm. We acknowledge the
504 generous support of the Kennedy Trust for Rheumatology Research, IDRM and Carl Zeiss
505 GMBH for the microscopy facilities (Zeiss 980) used in this research. We acknowledge the
506 generous support of the Kennedy Trust for Rheumatology Research and a Wellcome Trust
507 Multi-User Equipment Grant 202911/Z/16/Z for the microscope purchase (Zeiss 880
508 multiphoton) and facilities used in this research. We want to thank Dr Ida Parisi, Dr
509 BryonysStott and Miss Rhiannon Cook in the Kennedy Institute of Rheumatology Histology
510 Service for tissue processing and staining. We thank Angela Lee and Moustafa Attar in the
511 Oxford Genomics Centre at the Wellcome Centre for Human Genetics (funded by Wellcome
512 Trust grant reference 203141/Z/16/Z) for the generation and initial processing of sequencing
513 data. We also acknowledge the support received from Stijn van Dongen at the Wellcome
514 Sanger Cellular Genetics Informatics team and the Teichmann lab for discussion and support
515 with scripts.
516
517

518 YG was funded by a Wellcome Trust Clinical Research Fellowship (CRTF), grant reference
519 201224/Z/16/Z.

RB-C Grant 315307, Forskerprosjekt 2020, Researcher Project / International Mobility Grant from the Research Council of Norway and travel grant from the Per Brandtzæg's Fund for Research in Mucosal Immunology.
ET was supported by Wellcome Trust (095688/Z/11/Z and 212240/Z/18/Z, awarded to FP), Nuffield Department of Medicine, and MRC core grant reference MC_UU_00008.
FP was supported by Wellcome Trust (095688/Z/11/Z and 212240/Z/18/Z).

Competing interest statement

FP receives consultancy fees or research support from Janssen, GSK, T-Cypher and Novartis

In the past three years, S.A.T. has consulted or been a member of scientific advisory boards at Roche, Genentech, Biogen, GlaxoSmithKline, Qiagen and ForeSite Labs and is an equity holder of Transition Bio.